HIGH ALTITUDE DUST GLOBAL DISTRIBUTION, VERTICAL MIXING, AND PARTICLE SIZES DURING THE 2001 PLANET-ENCIRCLING DUST STORM. R. T. Clancy[1], M. J. Wolff[1], B. A. Whitney[1], M. D. Smith[2], and B. A. Cantor[3], [1]Space Science Institute, Boulder, CO, (Clancy@spacescience.org), [2]NASA Goddard Space Flight Center, Greenbelt, MD, [3]Malin Space Science Systems, La Jolla, CA.

Introduction: Dust aerosols are observed to extend to high altitudes during planetary-scale dust storms [1-4]. Most recent GCM modeling of vertically extensive dust loading over the course of such storms indicates that dust particles with radii of 1-2 μm may be lifted to altitudes above 40 km, and their vertical distributions strongly affected by vigorous meridional transport which is intensified by the resulting dust absorption of solar flux [5]. Here we present a multiple scattering, spherical radiative transfer (RT- [6]) analysis of Mars Global Surveyor (MGS) TES (Thermal Emission Spectrometer [7]) solarband bolometer and thermal infrared spectral limb observations, taken during the 2001 planet-encircling dust storm (starting around Mars solar longitude, L_s, 185° [8, 9]). The latitude-longitude distribution of TES solarband limb brightness at 60 km tangent altitudes is displayed versus L_s to illustrate the evolving global pattern of high altitude dust loading in the context of lower atmospheric dust lifting/dust columns. Retrievals for dust mixing ratio and particle size vertical profiles are performed for selected locations and periods.

TES Solarband and Thermal IR Limb Observations: TES limb observations provide vertical profiles of solar bolometric (0.3-3.0 μm, μ≈0.7 μm) and thermal IR spectral (6-50 mμ) radiance profiles with 10-15 km vertical resolution [7]. TES limb observations were obtained daily with coarse global mapping coverage (10-20° latitude, 30° longitude), and so characterize the three dimensional distribution of dust aerosol loading in the global Mars atmosphere versus time [8]. The combined visible/IR spectral coverage of TES limb observations further supports retrievals of dust and ice aerosol extinction opacity and particle size profiles [10]. Dust particle size constraints are limited for altitudes above 30 km (e.g., [11]), where variations associated with rapid gravitational settling rates are expected to be most important. Measurements of visible-to-IR dust opacity ratios, which have provided quatitative particle sizes for lower atmospheric dust columns [12-13], are essential for determinations of dust particle size profiles from TES limb observations.

Spherical RT analysis of TES Limb Observations: Combined RT analysis of TES solarband and thermal IR limb observations requires self-consistent spherical, multiple scattering treatment of atmospheric scattering and emission by dust aerosols. In concert with the monte carlo Mars RT code developed by Barb Whitney and Mike Wolff [6], we employ detailed spectral models of dust scattering/absorption based upon TES [14], Mars Exploration Rover mini-TES [15], and Mars Reconnaissance Orbiter CRISM [16] spectral dust analyses. These models include the results of Viking IRTM [17] and MGS TES [13] solarband emission-phase-function (EPF) empirical determinations of dust scattering phase functions, as well as numerical modeling of oblate disk-shaped particle scattering versus particle size [18].

Dust mixing ratio and particles size profiles are derived iteratively, to provide consistent profile fits to observed solarband bolometric and thermal IR spectral limb brightnesses. The observed IR spectrum of aerosol emission/scattering during the dusty, warm atmospheric period of the 2001 dust storm is dominated by dust, without detectable ice signatures for the six profiles modeled. We employ the thermal IR dust spectral indices derived from TES/mini-TES nadir/upward observations [14,15], which well fit the observed limb spectral shapes of IR emission/scattering. The dependence of the observed IR spectral shape with dust particle size is modest such that the primary size information is obtained from the observed ratio of solarband and thermal IR spectral brightness.

Limb observations over the lower 1-3 scales heights are generally saturated in that these lower altitudes are obscured by high slant paths of extinction above the tangent point. Consequently, we constrain the vertical columns of dust optical depth according to the TES nadir-derived 9 μm dust absorption optical depth database from Smith et al. [19]. The wavelength-dependent extinction column optical depth is then calculated from particle-size dependent dust scattering models. We adopt the TES tempertature profiles from the combined nadir-limb analysis of Conrath et al. [20], as well as surface brightness temperatures from the TES database.

Maps of TES Solarband Scattering at 60 km Altitude: Figures 1a-d present latitude-longitude contour maps of the TES solaband limb brightness at a 60 km tangent altitude, averaged over L_s intervals of 186-192°, 192-197°, 208-213°, and 217-223°. L_s intervals of 5-6° (10-11 days) are required for sufficient limb coverage to constrain adequately global average conditions, but they also lead to significant temporal averag-

ing of very large daily variability. Figure 1a corresponds to the first 1-2 weeks of the 2001 dust storm initiation, where peak brightness regions correspond roughly to region of maximum dust column optical depth [8] and active dust lifting at the surface [9]. Figures 1b and 1c present a dust-free corridor over 100-250W longitudes which persists over L_s=190-215° period, although detailed longitudinal and latitudinal boundaries for this feature vary considerably during the six week period. This behavior also conforms roughly with lower atmospheric dust behavior in that dust optical depths peak on either side of 200W.

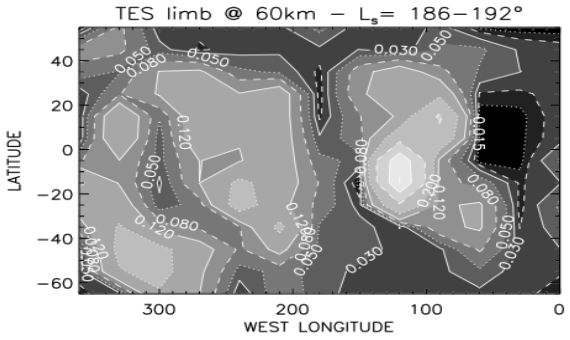

Fig 1a – The global distribution of Mars atmospheric solarband limb brightness, associated with dust scattering at a tangent altitude of 60 km, for the L_s=186-192° period of dust storm development.

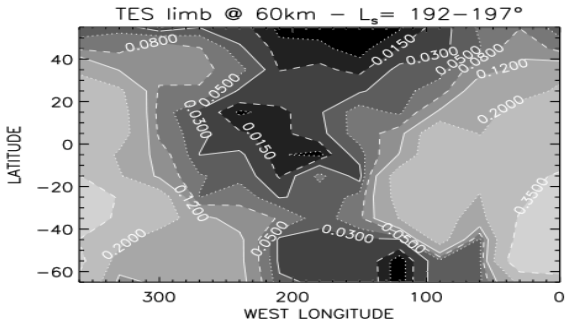

Fig 1b- same as for fig 1a, for the L_s interval 192-197°.

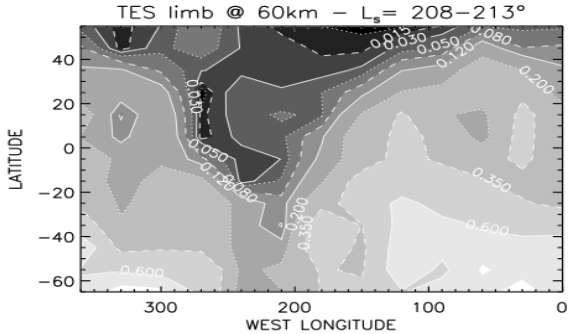

Fig 1c- same as for fig 1a, for the L_s interval 208-213°.

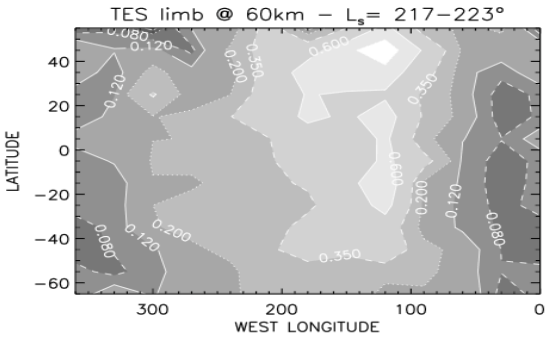

Fig 1d- same as for fig 1a, for the L_s interval 217-223°.

After L_s 215°, the global distribution of dust scattering at 60 km altitudes evolves rapidly towards greater longitudinal uniformity and reversal of high southern latitude maximum dust loading towards a northern mid-latitude maximum in dust loading. Although qualitatively similar, these temporal behaviors in high altitude dust loading present much stronger longitudinal, latitudinal, and daily variations than lower atmospheric dust columns. They are also accompanied by vertical gradients in dust mixing that reflect large-scale horizontal transport, rather than one-dimensional (local) vertical transport of dust.

TES Solarband Radiance Profiles: TES limb solarband limb radiance profiles for separate longitudes of 16W and 174W at low southern latitudes 3S and 13S, respectively, are presented in figure 2. Plotted square and asterisk symbols represent observed TES radiances (in reflectance I/F units) as compared to dashed and solid line best-fit RT model radiances. The large difference in upper atmospheric dust loading between the two longitudes corresponds with the large-scale longitudinal variation presented in figure 1d. The distinctive "kink" in the 174W limb radiance profile above 50 km is associated with an altitude-increasing dust mixing ratio, rather than potential clouds, as indicated by the associated thermal IR limb spectra for these TES limb observations (Figures 3 ab).

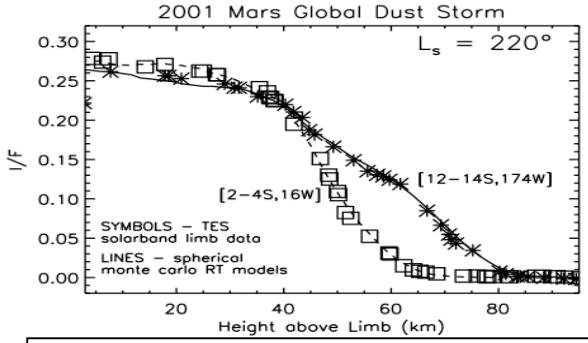

Fig 2- TES solarband limb brightness profiles for separate longitudes of 16W (data-squares, RT model-dashed line) and 174W (data-asterisks, RT model-solid line). Both longitudes correspond to atmospheric dust scattering over low southern latitudes at L_s=220°.

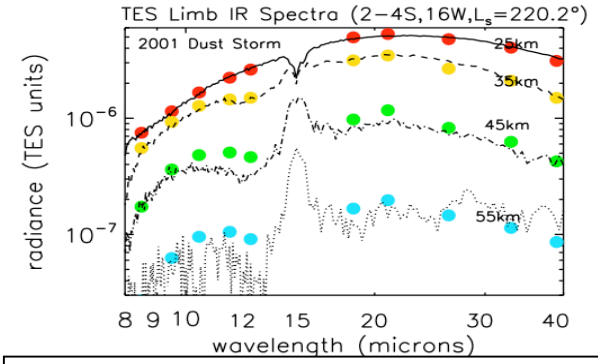

Fig 3a- Observed (lines) versus RT modeled (colored circles) limb thernal IR spectral radiances versus limb tangent altitude (as labeled) for the 3S, 16W TES observation associated with the solarband limb radiance profile of figure 2 (dashed line, squares).

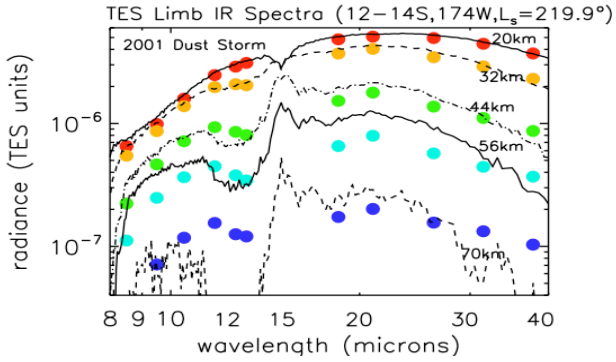

Fig 3b- same as figure 3a, for the 13S, 174W TES observation associated with the solarband limb radiance profile of figure 2 (solid line, asterisks).

TES Solarband Radiance Profiles: TES thermal IR limb spectra in figure 3ab are presented by varying linestyles as a function of limb tangent altitude (as labeled in the figures), in TES radiance units (Wcm^{-2}str^{-1}/cm^{-1}). Apart from the molecular CO_2 line at 15 μm, which appears in emission above ~30 km latitudes, the observed emission/scattering is contributed by atmospheric dust. No detectable ice aerosol contribution at 12 μm appears at either location. The colored circles indicate RT modeled radiances calculated for a discrete set of wavelengths that characterize the broadband IR spectrum of atmospheric dust. The dust total optical depth, vertical mixing profile, particle size distribution, and optical constants associated with these model spectra corresponds to the same dust parameters incorporated in the solarband limb radiance models presented in figure 2. Visible and thermal IR wavelength dependences for the dust optical constants, optical depth, and single scattering phase functions are based upon the physical dust model (size, shape, optical indices) as desribed earlier. The solution dust mixing profiles and particle sizes are indicated in the following sections.

Derived Dust Mixing Profiles: Dust mixing ratio profiles for the limb observations/models presented in figures 2 and 3ab are shown in figures 4ab. The best-fit dust mixing profile is represented by the diamond symbols and compared to one-dimensional model profiles (dashed and dotted lines), where dust gravitational settling is balanced by vertical eddy mixing [21]. Variations in the Conrath parameter (ν) would correspond to variable dust particle sizes and eddy diffusion rates.

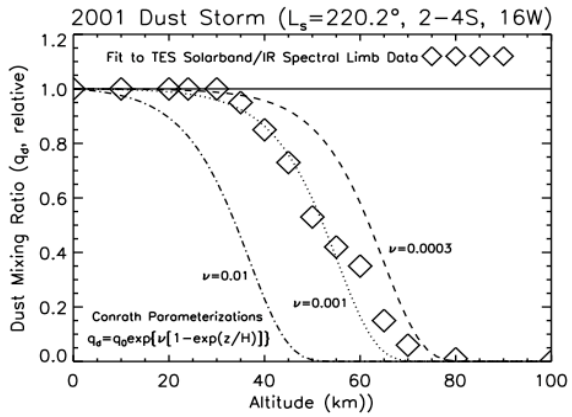

Fig 4a- Best-fit dust mixing profile (diamonds) versus Conrath parameterization models for the 3S, 16W TES limb observations of figures 2 and 3a.

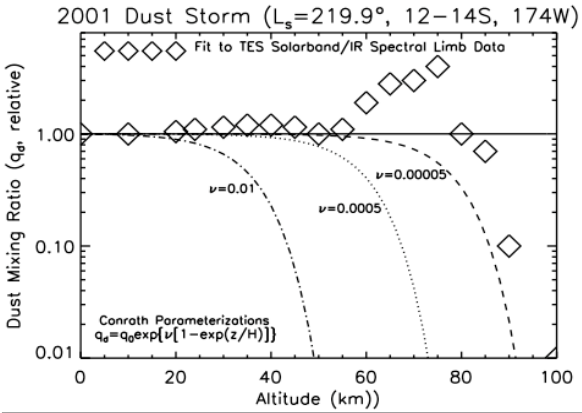

Fig 4b- same as figure 4a, for the TES 13S, 174W limb observations of figures 2 and 3b. Notice the vertical scale in this case is logarithmic, to display the several hundred percent increase in mixing ratios from 60 to 80 km.

Clearly dust was transported to very high altitudes (70-80 km) over the course of this 2001 dust storm, and often exhibits altitude increasing mixing ratios

above 40 km for regions/times during which dust loading above 50 km is most prominent. This behavior implies a meridional transport source of dust from (presumably) southern latitudes at altitudes of or above the altitudes of peak mixing ratios. Kahre et al. [5] predict such behavior on the basis of MGCM dust storm simulations, although at lower altitudes (≤ 40 km) than indicated in figure 4b. The existence such altitude increasing dust mixing ratios is inconsistent with a one-dimensional model such as employed by Conrath [21], which was developed to model the temporal decline of 0.3 mbar atmospheric temperatures observed by Mariner 9 during the decay of the 1971 planet-encircling dust storm. However, the conclusion that dust loading extended to above 50 km during this 2001 storm, associated with the constraint that $\nu \leq 0.01$ is quite consistent with the current analysis of the 2001 dust storm.

Derived Dust Particle Sizes: The primary sensitivity to dust particle sizes in the analysis is the ratio of visible to thermal IR opacity, which increases rapidly with decreasing particle size for the micron-sized particles typical of the martian atmophere [12,13]. The solarband/thermal IR model fits of figures 2 and 3 incorporate dust particle sizes of 1.5 μm (effective, cross-section-weighted radius for a modified gamma size distribution with a variance of 0.4 μm). Smaller dust particle sizes (e.g., 1 um radii) underpredict the observed thermal IR radiances above 30 km (i.e., above limb transmissions >>1) by factors of two or more. In fact, a best fit to model-data thermal IR limb radiances above 40 km in figure 3b requires a dust particle radius of 2 μm rather than for the value of 1.5 μm presented. Such large particle sizes appear reasonably consistent with the model predictions of Kahre et al. [5] for altitudes as high as 50 km, but probably not as high as 70 km, as implied by conditions sampled in figure 3b. It is worth noting that the maintenance of longitudinal corridors of dust-free upper atmospheric conditions (figure 1) implies large dust particle sizes (rapid gravitational settling rates), given that zonal winds should transport dust into these corridors over significantly less than 1 day timescales.

Conclusions: Dust was suspended to altitudes as high as 80 km during the 2001 planet-encircling dust storm, exhibiting extreme longitudinal variations that qualitatively correlate with longitudinal variation in surface dust lifting and atmospheric dust column. Derived dust mixing profiles often exhibit altitude increasing values over 40-70 km altitudes, indicative of significant meridional transport effects at or above these altitudes. Derived dust particle sizes at altitudes above 40 km are comparable to those characterizing the lower atmosphere (≥1.5 μm effective radii), indicating very strong vertical transport rates that may be compared, in the context of implied meridional transport rates, through future MGCM dust storm simulations.

References: [1] Anderson E. M. and Leovy C. B. (1978), *J. Atmos. Sci., 35*, 1861–1883. [2] Jaquin F., et al. (1986) *Icarus, 68*, 442–461. [3] Smith M. D. (2003), *Proc. Sixth International Conf. on Mars*, Abstract #3174*, Pasadena*, CA. [5] Kahre M. A. et al. (2008), *Icarus, 195*, 576-597. [6] Whitney B. A. et al. (1999), *Proc. Fifth International Conf. on Mars,, Pasadena*, CA. [7] Christensen P. R. et al. (1992) *JGR, 97*, 7719–7734. [8] Smith M. D. et al. (2002) *Icarus, 157*, 259–263. [9] Cantor B. A. (2007) *Icarus, 186*, 60–96. [10] Clancy R. T., et al. (2007) *JGR, 112,* EO4O04. [11] Chassefiere E. et al. (1992) *Icarus, 97*, 46–69. [12] Martin T. Z. (1986) *Icarus, 66*, 2–21. [13] Clancy R. T. et al. (2003) *JGR, 108*, E9 5098. [14] Wolff M. J. and R. T. Clancy (2003) *JGR, 108*, E9 5097. [15] Wolff M. J. et al. (2006) *JGR, 111*, E12S17. [16] Wolff M. J. et al. (2007) *AGU Fall Meeting*, Abstract #P31D-03. [17] Clancy R. T. and S. W. Lee (1991) *Icarus, 93*, 135–158. [18] Mishchenko, M. I. et al. (1996) *JQSRT, 55*, 535–575. [19] Smith M. D. et al. (2004) *Icarus, 167*, 148–165. [20] Conrath B. J. et al. (2000) *JGR, 105*, 9509–9520. [21] Conrath B. J. (1975) *Icarus, 24*, 36–46.